Journal of Power Sources 195 (2010) 2431–2442

Contents lists available at ScienceDirect

Journal of Power Sources

journal homepage: www.elsevier.com/locate/jpowsour

Review

Advanced materials for sodium-beta alumina batteries: Status, challenges and perspectives

Xiaochuan Lu, Guanguang Xia, John P. Lemmon, Zhenguo Yang*

Pacific Northwest National Laboratory, Richland, WA 99352, USA

ARTICLE INFO

Article history:
Received 1 October 2009
Received in revised form
15 November 2009
Accepted 25 November 2009
Available online 2 December 2009

Keywords:
Sodium-beta alumina battery
β''-Al_2O_3 electrolyte
Molten sodium
Sulfur
Transition metal chlorides

ABSTRACT

The increasing penetration of renewable energy and the trend toward clean, efficient transportation have spurred growing interests in sodium-beta alumina batteries that store electrical energy via sodium ion transport across a β''-Al_2O_3 solid electrolyte at elevated temperatures (typically 300–350 °C). Currently, the negative electrode or anode is metallic sodium in molten state during battery operation; the positive electrode or cathode can be molten sulfur (Na–S battery) or solid transition metal halides plus a liquid phase secondary electrolyte (e.g., ZEBRA battery). Since the groundbreaking works in the sodium-beta alumina batteries a few decades ago, encouraging progress has been achieved in improving battery performance, along with cost reduction. However, there remain issues that hinder broad applications and market penetration of the technologies. To better the Na-beta alumina technologies require further advancement in materials along with component and system design and engineering. This paper offers a comprehensive review on materials of electrodes and electrolytes for the Na-beta alumina batteries and discusses the challenges ahead for further technology improvement.

Contents

* Corresponding author at: Pacific Northwest National Laboratory, Materials Science, 902 Battelle Blvd, P.O. Box 999, K2-44, Richland, WA 99352, USA.
Tel.: +1 509 375 3756; fax: +1 509 375 2186.
E-mail address: Zgary.Yang@pnl.gov (Z. Yang).

0378-7753/$ – see front matter © 2009 Published by Elsevier B.V.
doi:10.1016/j.jpowsour.2009.11.120

1. Introduction

Environmental concerns over the use of fossil fuels and their resource constraints, along with the trend of carbon monetization, have spurred increasing use of energy generated from renewable sources such as wind and solar. Despite the abundance and ready availability, solar and wind power are variable and uncontrolled. An effective approach to smooth out the intermittency and make it dispatchable is to use electrical energy storage (EES), storing excessive energy and releasing it when needed. The EES technologies are also demanded to improve the reliability and efficiency of future grids, which are expected to be able to provide fuel (i.e., electricity) for plug-in hybrid vehicles and allow for two-way communication and digital balancing of demand and supply (i.e., smart grid). Among various EES technologies, electrochemical energy storage systems or batteries are capable of reversibly storing and releasing electrical energy without involving "Carnot" cycles, thus potentially allowing a high efficiency. One such technology is based on a solid electrolyte membrane that selectively allows sodium ion transport between a positive and negative electrode. As the most widely used solid electrolyte has been based on beta alumina, this type of electrochemical devices is often referred as Na-beta batteries (NBBs). Due to the high round-trip efficiency, high energy density and capability of energy storage for duration of hours, the NBB technologies have been increasingly interested for renewable storage and utility applications, as well as for clean, efficient vehicles [1]. Significant progress has been achieved in the NBB technologies during the past few decades. However, the batteries are still facing challenges in battery performance and cost for broad market penetration. Advancement in the technologies closely relies on the development and use of advanced materials that make battery components. This paper provides an overview on NBBs, including the basic electrochemistries and materials for various cell components, while exploring future direction in material research and development for further battery performance improvement and cost reduction.

2. Basic electrochemistries

NBBs reversibly charge and discharge electricity via sodium ion transport across a β″-Al_2O_3 solid electrolyte (or, BASE) that is typically doped with low valence elements. For minimum electrical resistance and satisfactory electrochemical activities, the NBBs usually operate at moderate temperatures (300–350 °C). With a melting point (MP) at 98 °C, the sodium in anodes (negative) is thus in a molten state. A common cathode (positive) is molten S/Na_2S_x (MP of S = 115 °C) and porous graphite felts are usually incorporated into the cathode to improve its electrical conductivity. This type of battery is known as sodium–sulfur (Na–S) battery. The ground breaking work was carried out by Ford Motor Company in the late 1960s [2]. Since then, the NBBs have been commonly constructed in tubular designs, as schematically shown in Fig. 1. The half- and overall-cell reactions are as follows:

$$\text{Anode}: \quad 2\text{Na} \Leftrightarrow 2\text{Na}^+ + 2\text{e}^- \tag{1}$$

$$\text{Cathode}: \quad x\text{S} + 2\text{Na}^+ + 2\text{e}^- \Leftrightarrow \text{Na}_2\text{S}_x \tag{2}$$

$$\text{Overall-cell reaction}: \quad x\text{S} + 2\text{Na} \Leftrightarrow \text{Na}_2\text{S}_x \quad (x = 5\text{–}3), \quad E = 2.08\text{–}1.78\ \text{V at } 350\ ^\circ\text{C} \tag{3}$$

A closely-related system is the ZEBRA ("ZEolite Battery Research Africa") battery that uses β″-Al_2O_3 electrolyte to separate a molten sodium anode and metal halide cathode [3]. The solid-state halide electrode is added with a molten secondary electrolyte (e.g., $NaAlCl_4$) to allow rapid transport of sodium ions. If nickel chloride is used as cathode material, the cell reactions are as follows:

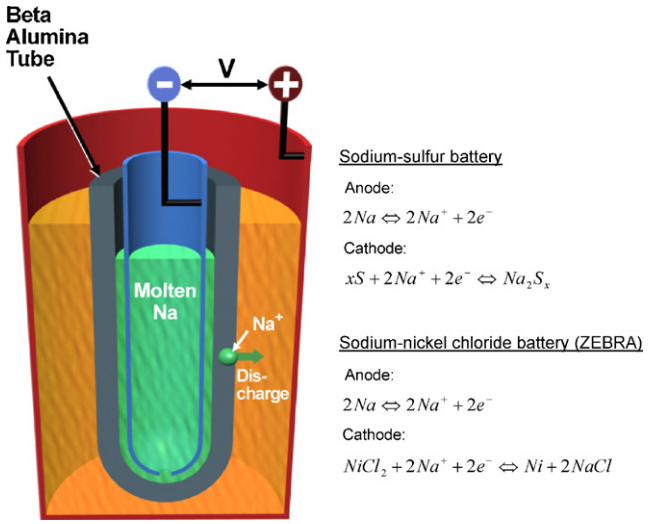

Fig. 1. Single-cell and tubular design of a sodium/nickel chloride battery and electrode reactions.

$$\text{Anode}: \quad 2\text{Na} \Leftrightarrow 2\text{Na}^+ + 2\text{e}^- \tag{4}$$

$$\text{Cathode}: \quad \text{NiCl}_2 + 2\text{Na}^+ + 2\text{e}^- \Leftrightarrow \text{Ni} + 2\text{NaCl} \tag{5}$$

Overall-cell reaction :

$$\text{NiCl}_2 + 2\text{Na} \Leftrightarrow \text{Ni} + 2\text{NaCl}, \quad E = 2.58\ \text{V at } 300\ ^\circ\text{C} \tag{6}$$

During discharge, metallic sodium (anode) is oxidized at the sodium/β″-Al_2O_3 interface to form sodium ions, which is same as that in Na–S battery. The Na^+ ions are transported through the electrolyte membrane as well as molten secondary electrolyte and combine with nickel chloride in the cathode (Eq. (5)). The nickel chloride is then reduced to Ni metal. During charge, these reactions are reversed. An electrochemical cell can be assembled in one of three states: discharged state, charged state and partially charged state. Considering that both anhydrous nickel chloride and metallic sodium are rather difficult to handle, the cell is typically assembled in the discharged state. A mixture of metallic nickel and sodium chloride powders is filled into the cathode chamber and sodium as well as nickel chloride are generated during the first charge [4,5].

3. β″-Al_2O_3 solid electrolyte (BASE)

3.1. Crystal structure

The beta alumina group of oxides is characterized by structures of alternating closely-packed slabs and loosely-packed layers. The loosely-packed layers, which contain mobile sodium ions, are called conduction planes. In these conduction planes, sodium ions are free to move under an electric field. The closely-packed oxide slabs are comprised of four layers of oxygen ions with aluminum ions in both octahedral and tetrahedral interstices. These layers, referred as a spinel block, are bonded to two neighboring spinel blocks via conduction planes. There are two distinct crystal structures in the group: β-Al_2O_3 (hexagonal; $P6_3/mmc$; $a_o = 0.559$ nm, $c_o = 2.261$ nm) [6,7] and β″-Al_2O_3 (rhombohedral; $R3m$; $a_o = 0.560$ nm, $c_o = 3.395$ nm) [8,9]. They differ in chemical stoichiometry, stacking sequence of oxygen ions across the conduction plane (see Fig. 2) and sodium ion conductivity. As shown in Fig. 2, a conduction plane in the β-Al_2O_3 is sandwiched between

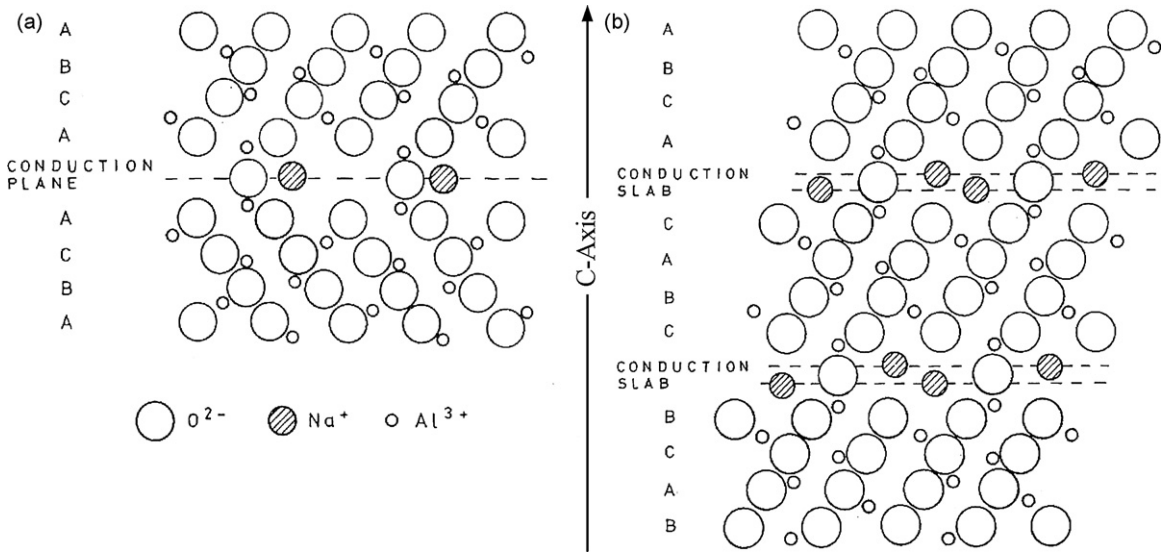

Fig. 2. Projection of (a) β-Al_2O_3 and (b) β″-Al_2O_3 unit cells on (1 1 $\bar{2}$ 0) showing stacking sequence [12].

two spinel blocks while it is two conduction slabs separated by three spinel blocks in the β″-Al_2O_3. Due to the difference in oxygen stacking sequence, the unit cell of β″-Al_2O_3 is 50% larger than that of β-Al_2O_3. β″-Al_2O_3 exhibits a higher sodium ionic conductivity (typically 0.2–0.4 S cm^{-1} at 300 °C [10,11]) and is the preferred phase for sodium battery electrolyte applications.

Fig. 2a shows stoichiometric β-Al_2O_3 with the formula $(Na_2O)_{1+x}11Al_2O_3$ ($x=0$). In practical, x could be as high as 0.57 for undoped β-Al_2O_3 [12]. Accommodation of excessive sodium atoms in the interstitial sites could significantly improve the conductivity. In the presence of such excessive sodium ions, electrical compensation might be achieved via two mechanisms. The first one is so-called "Frenkel defects" mechanism [13,14], in which an interstitial oxygen ion in one of the three equivalent mid-oxygen sites in the conduction plane is assumed to be stabilized by the occurrence of an interstitial aluminum ion, and the interstitial aluminum ion itself is compensated by vacancy in a normal octahedral aluminum site. The presence of each interstitial oxygen ion allows two extra sodium ions into the plane. The second one is substitution of aluminum ions in the spinel blocks with mono or divalent ions (e.g., Li^+, Co^{2+} and Mg^{2+}). Compared to the first one, this mechanism allows significant departure from stoichiometry and is probably the only approach to obtain ion-rich single crystal. With Mg^{2+} doping, the maximum value of x in $(Na_2O)_{1+x}11Al_2O_3$ could increase from 0.57 to 0.67 [12]. In the case of doped β-Al_2O_3, the structure change to β″-Al_2O_3 offers accommodation of higher levels of sodium ions, which further improves the ionic conductivity. It has been reported that conductivity of ion-rich β-Al_2O_3 is much higher compared to usual β-Al_2O_3 while that of β″-Al_2O_3 is slightly higher than the ion-rich one [15]. The β″-Al_2O_3 tends to decompose at elevated temperatures (e.g., higher than 1600 °C) unless stabilized by the mono or divalent dopant ions. The ideal compositions of β″-Al_2O_3 are $Na_{1.67}Al_{10.33}Mg_{0.67}O_{17}$ (Mg^{2+} doped) and $Na_{1.67}Al_{10.67}Li_{0.33}O_{17}$ (Li^+ doped) [12].

3.2. Powder synthesis

β″-Al_2O_3 powders can be synthesized by conventional solid-state reaction [10,16–18], sol–gel process [19–24], co-precipitation technique [21,25], spray-freeze/freeze-drying method [26,27], etc. The preparation of β″-Al_2O_3 via a solid-state reaction is typically carried out with the starting materials of α-Al_2O_3; Na_2O added as Na_2CO_3, $NaNO_3$, NaOH or $NaAlO_2$; and a small amount of MgO as $Mg(NO_3)_2$ or itself and/or Li_2O as Li_2CO_3, LiOH or $Li_2O{\cdot}5Al_2O_3$. The procedures involve multiple ball-milling and calcination steps, followed by final sintering treatment above 1600 °C. Disadvantages of the process include: (i) sodium loss and exaggerated grain growth during the high-temperature sintering. The extensive grain growth can lead to significant reduction in mechanical properties (to be discussed in Section 3.4); (ii) remnant $NaAlO_2$ along grain boundaries, which results in sample moisture sensitive; and (iii) formation of two-phase mixture (β- and β″-Al_2O_3) with relatively low conductivity. In order to maximize the amount of β″-Al_2O_3, a number of techniques have been employed, including post-sinter annealing [28], two-peak firing schedule [29], so-called Zeta process [30] and seeding of reaction mixture with pre-reacted β″-Al_2O_3 [28]. All the processes require high purity Al_2O_3 precursors and a long period of time at very high temperatures. Compared to the solid-state reaction route, the solution-based chemical methods offer several advantages: (i) producing powders with a higher degree of homogeneity and therefore high purity final products; and (ii) yielding high surface area powders that can be sintered at relatively low temperatures. The synthesis of β″-Al_2O_3 via the chemical methods have the drawback of coexistence of β″-Al_2O_3 with β-Al_2O_3 as well [19,22,24].

As attractive alternatives to the high purity chemical precursors, cheap abundant raw materials from hydroxyl alumina group such as boehmite and bayerite could be used to prepare pure β″-Al_2O_3 [31,32]. For example, it was synthesized with the starting precursors of boehmite, Na_2CO_3 and Li_2CO_3 via the solid-state reaction. The pure β″-Al_2O_3 was obtained at temperatures as low as 1200 °C without α-Al_2O_3, $NaAlO_2$, or β-Al_2O_3 side products. According to models proposed by Poulieff et al. [33] and Vanzyl et al. [31], the oxygen stacking sequence of the Al_2O_3 precursor is inherited by the final product and pure β″-Al_2O_3 can be formed with a commercial precursor material with a similar oxygen sublattice. Both boehmite and bayerite have highly crystalline and ordered structures and after dehydration, they form a transition γ-Al_2O_3 structure, which is characterized with a regular cubic closely-packed oxygen array. During formation of β″-Al_2O_3, the oxygen ions from Na_2O and Li_2O components are inserted between the closely-packed layers to provide bridging oxygen ions, as shown in Fig. 3. The introduction of bridging oxygen ions imparts an overall negative charge into the γ-Al_2O_3 structure, which, therefore, permits the diffusion of lithium ions into the defected spinel blocks. The lithium ions act as "pins" that stabilize the cubic closely-packed oxygen spinel blocks. Mean-

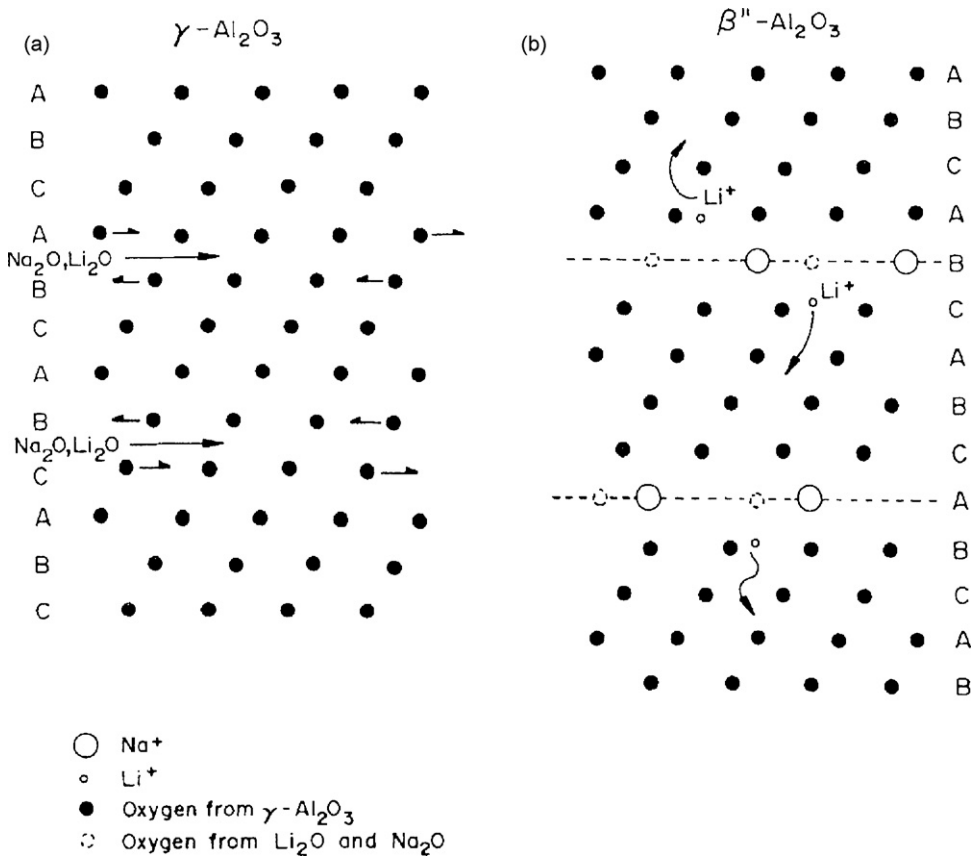

Fig. 3. Schematic illustration of the proposed mechanism for the conversion of oxygen lattice of (a) γ-Al_2O_3 to (b) β''-Al_2O_3 [31].

while, since sodium ions are too large to diffuse into the spinel blocks, they remain in the conduction plane. The use of commercial boehmite precursor to prepare β''-Al_2O_3 significantly reduces the sintering temperature and therefore, alleviates sodium loss during the process.

3.3. BASE fabrication

The as-synthesized powders are ball-milled to desired particle size and then sintered into required shapes, disc or one-end closed tube depending on cell design, by either isostatic pressing, electrophoretic deposition, slip casting or extrusion techniques [12]. Isostatic pressing is a relatively simple, well-established and cost-effective method, in which powders are introduced into a polyurethane mold and compacted by applying a hydraulic pressure to the mold. The powders are pressed isostatically to a relatively high density with a good dimensional tolerance. Another advantage of the method is high production rate. Electrophoretic deposition [34,35] uses an electrically charged mandrel placed in a dielectric liquid with β''-Al_2O_3 powder as the suspension in the liquid. An electric field is applied between the mandrel and a counter electrode, and powders are deposited uniformly onto the mandrel. The green tube is removed from the mandrel and further isostatically pressed to improve the homogeneity and strength. Slip casting is another technique to fabricate β''-Al_2O_3 electrolyte. Byckalo et al. [36] casted β''-Al_2O_3 using aqueous suspensions with additives in plaster molds to produce green tubes with a relatively high density. Rivier and Pelton [37] slip-casted β''-Al_2O_3 in a similar way but employed a different kind of mold. The main drawback of slip casting lies in that there is a strong particle orientation in the cast product (parallel to the tube wall) and the low resistivity direction is perpendicular to the direction of current flow. The final product thus exhibits a higher resistance. In order to increase production rate, Ford Motor Company developed an extrusion technique to produce β''-Al_2O_3 tubes [38]. The apparatus is composed of a fixed mandrel over which a moveable die is pushed and, thus, the powders between the two components are compressed.

After removal from the mold, the green body is ready for high-temperature sintering treatment to achieve a high density, adequate mechanical strength and good electrical performance. Several issues need to be addressed during the sintering process. The first one is sodium evaporation at high temperatures, as mentioned earlier. It can be simply controlled by encapsulation sample in a platinum or magnesia container. One technique, zone sintering, also can be employed to minimize the sodium loss by shortening dwelling time in the high-temperature zone [39,40]. The green tube is rapidly passed through the hot zone without encapsulation and the resulting product exhibits a satisfactory density and microstructure. The second issue is duplex microstructure consisting of large grains (50–500 μm) in a fine-grained matrix (grain size $\leq$ 10 μm) after sintering [10,11,29]. The exaggerated grain growth may be suppressed with a short period of sintering at high temperatures (<30 min). The third issue is lower β''-Al_2O_3 conversion rate, which can be resolved via the techniques mentioned in Section 3.2 or by using boehmite as the precursor. As an example, Fig. 4a shows the XRD results of β''-Al_2O_3 powders synthesized from boehmite precursor. It can be seen that a pure β''-Al_2O_3 phase is yielded after fired at temperatures as low as 1200 °C, which is in agreement with literatures. The powders are then attrition-milled, pelletized by die-pressing uniaxially at 8000 psi and further isostatically pressed at 50,000 psi. The green pellet is finally sintered at 1600 °C for 30 min in the air. The microstructure of the pellet after thermal etching is shown in Fig. 4b. Extremely large rod-like grains are observed in the fine-grained matrix while the density is

Table 1
Physical and mechanical properties of β″-Al_2O_3 fabricated via various methods.

Property	Fabrication condition						
	Isostatically pressed at 60,000 psi and sintered at 1585 °C for 30 min	Isostatically pressed at 60,000 psi and sintered at 1585 °C for 20 min	Isostatically pressed and sintered at 1585 °C for 10 min	Isostatically pressed and sintered at 1605 °C for 20 min	Hot-pressed at 1400 °C for 15 min and annealed at 1300 °C for 20 h	Hot-pressed at 1400 °C for 15 min and annealed at 1400 °C for 24 h	Hot-pressed at 1400 °C for 15 min and annealed at 1500 °C for 24 h
Grain size (μm)	≈3	40% ≈3, 60% ≈90	65% ≈3, 35% ≈22	Duplex structure with large grain ≈120	<4	<5	200–300
Density (%)	≈98	≈97	95–97	≈97	>99	>99	>99
Fracture strength (MN m^{-2})	210	120	140–170	120	200	260	120
Critical stress intensity factor (MN m$^{-3/2}$)	2.3	2.8	–	2.6–3.8	2.3–3.8	3.6	2.6–4.0
Young's modulus (N m^2)	1.4×10^{11}	1.2×10^{11}	–	–	–	2.9×10^{11}	–
Reference	[57]	[57]	[58]	[59]	[59]	[57]	[59]

only 93% of theoretical density. Clearly, the fabrication of β″-Al_2O_3 electrolyte with a dense and fine-grained microstructure is rather difficult.

As an alternative method to the aforementioned, a vapor phase approach was developed by Virkar et al. [41–43], that offers a number of advantages. In the vapor phase process, the starting materials are high purity α-Al_2O_3 or α-Al_2O_3/YSZ (yttria-stabilized zirconia). The powders are ball-milled, pelletized and fired at 1600 °C in air to achieve a full density (>99%). The sample is then buried in packing powders (β″-Al_2O_3, prepared separately) and heat-treated at high temperatures (e.g., 1450 °C) in air for a period of time. The conversion occurs by coupled transport of sodium and oxygen ions from the packing β″-Al_2O_3 powders into the α-Al_2O_3 sample. As a good oxygen-ionic conductor, the added YSZ acts as fast oxygen conducting path to accelerate the conversion reactions. The addition of YSZ into α-Al_2O_3 enhances the mechanical strength as well, which will be discussed later. Advantages of the method include: (i) full conversion of α-Al_2O_3 to β″-Al_2O_3; (ii) elimination of the need of encapsulation as the conversion temperature is lower than that in the conventional process; (iii) grain size in the same level as that prior to conversion [43], as seen in Fig. 5; and (iv) resistance to moisture attack.

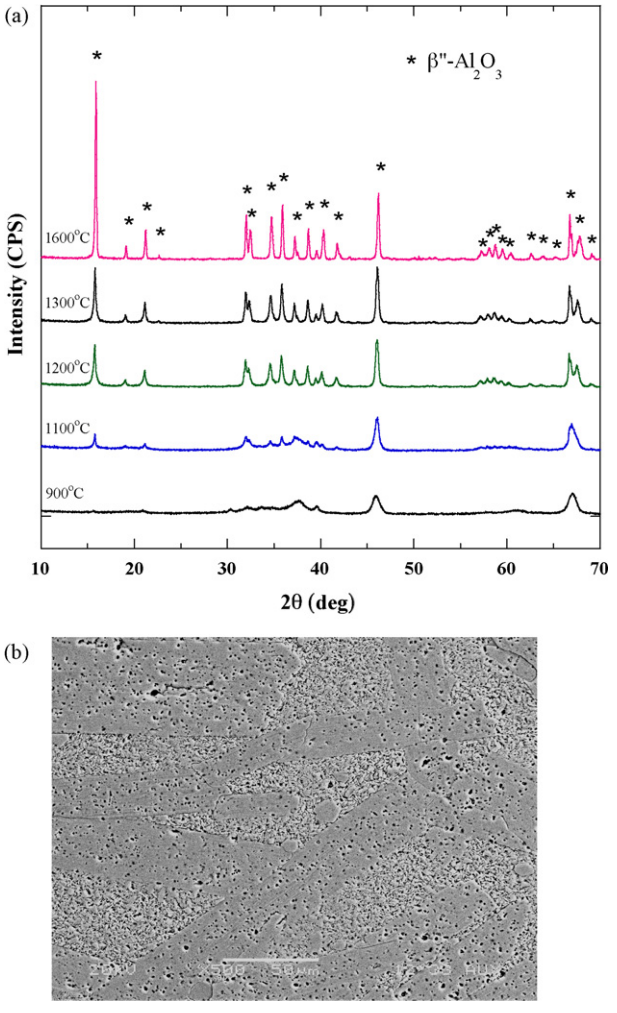

Fig. 4. (a) XRD patterns of synthesized β″-Al_2O_3 powders at various temperatures and (b) SEM image of β″-Al_2O_3 electrolyte after thermal etching.

3.4. Mechanical properties

The mechanical parameters of β″-Al_2O_3 fabricated via various methods are compared in Table 1. It can be seen that the strength is strongly affected by the microstructure (e.g., porosity and grain size). Dense β″-Al_2O_3 with an average grain size less than 10 μm exhibits much higher fracture strength (e.g., >200 MN m^{-2}), while that of completely coarse-grained ones with grain size larger than 200 μm is as low as 120 MN m^{-2}. The strength with a duplex structure varies from 120 to 170 MN m^{-2}, depending on the size and amount of large grain in the matrix. Also, the listed data indicates that high strength can be achieved with hot-pressed materials. When post-annealed at temperatures below 1500 °C, fine-grained electrolyte with a relative density above 99% can be obtained, which leads to fracture strength higher than 200 MN m^{-2}.

In addition to the abnormally large grains, defects such as pores, cracks and impurities may also significantly affect the mechanical strength of β″-Al_2O_3. The discrete pores, localized groups of smaller pores, micro- and macro-cracks, as well as impurities due to the local inhomogeneities in the powders may act as sites for crack initiation and propagation, which causes ceramic failure well below its fracture strength.

It has long been known that strength and fracture toughness can be enhanced by incorporation of ZrO_2 into β/β″-Al_2O_3 matrix [17,44–49]. The enhancement in fracture toughness (K_{IC}) leads to obvious improvement in critical current density (i_{cr}) [50], which has significant economic advantages with regard to battery performance. For example, not only the battery life would be extended, but the charging time could be dramatically shortened due to the

Table 2
Physical and mechanical properties of β''-Al_2O_3/ZrO_2 composite.

Property	Composition						
	β''-Al_2O_3 + 15 vol% ZrO_2 (doped with 3 mol% Y_2O_3)	β''-Al_2O_3 + 15 wt% ZrO_2	β''-Al_2O_3 + 25 wt% ZrO_2	β''-Al_2O_3 + 15 vol% ZrO_2 (doped with 2.4 mol% Y_2O_3)	β''-Al_2O_3 + 15 vol% ZrO_2 (doped with 6.6 mol% Y_2O_3)	β''-Al_2O_3 + 15 vol% ZrO_2	β''-Al_2O_3 + ZrO_2 or partially stabilized ZrO_2
Density (%)	≈97	≈97	≈97	>97	>97	≈97	–
Fracture strength ($MN\,m^{-2}$)	350	228–310	379	335	226	356	350
Critical stress intensity factor ($MN\,m^{-3/2}$)	4.5	5.0–8.0	5.0–8.0	4.1	3.2	4.1	4.0
Resistivity at 300 °C (Ω cm)	7.7	<7	–	8.5	–	9	–
Reference	[44]	[45]	[45]	[48]	[48]	[17]	[49]

increase of charging current density (during charge, degradation of ceramic electrolyte usually occurs when current density exceeds i_{cr}). Table 2 lists mechanical properties of various β''-Al_2O_3/ZrO_2 composites. Even though the relative density of ZrO_2-incorporated β''-Al_2O_3 is not as high as that of pure β''-Al_2O_3 (see Table 1), mechanical strength of the former is much higher than the latter. The typical fracture strength value of β''-Al_2O_3 with the addition of ZrO_2 is above $300\,MN\,m^{-2}$, which is almost 50% higher compared to that of pure β''-Al_2O_3 ($\sim 200\,MN\,m^{-2}$). The strengthening effects of ZrO_2 addition may result from several mechanisms, including transformation toughening [17,44,45,47,48], deflection toughening [47] and microstructure optimization [17,48,49]. In the transformation toughening, partially stabilized tetragonal ZrO_2 particles would convert to monoclinic polymorph at the tip of a propagating crack. Volume expansion associated with the phase transformation leads to formation of compressive stress, resulting in an increased resistance to crack propagation. Binner and Stevens [47] suggested that an additional proportion of improvement in the strength may result from deflection toughening mechanism, in which ZrO_2 particles act as a second phase to hinder crack propagation. According to Green [48], the strengthening of β''-Al_2O_3 was a combination of transformation toughening and microstructure optimization. The addition of both partially and fully stabilized (tetragonal and cubic, respectively) ZrO_2 into the matrix limited β''-Al_2O_3 grain growth and suppressed formation of abnormal grains, which led to improvement in strength and toughness. Heavens [49] insisted that the addition of unstabilized ZrO_2 into β''-Al_2O_3 can yield similar strength as that of partially stabilized ZrO_2, indicating that microstructure control instead of transformation toughening was the primary mechanism. Overall, the toughening effect of β''-Al_2O_3 by ZrO_2 seems rather complicated, depending on a number of factors such as composition, synthesis/processing method as well as microstructure, and one or multiple mechanisms discussed above may be responsible for it.

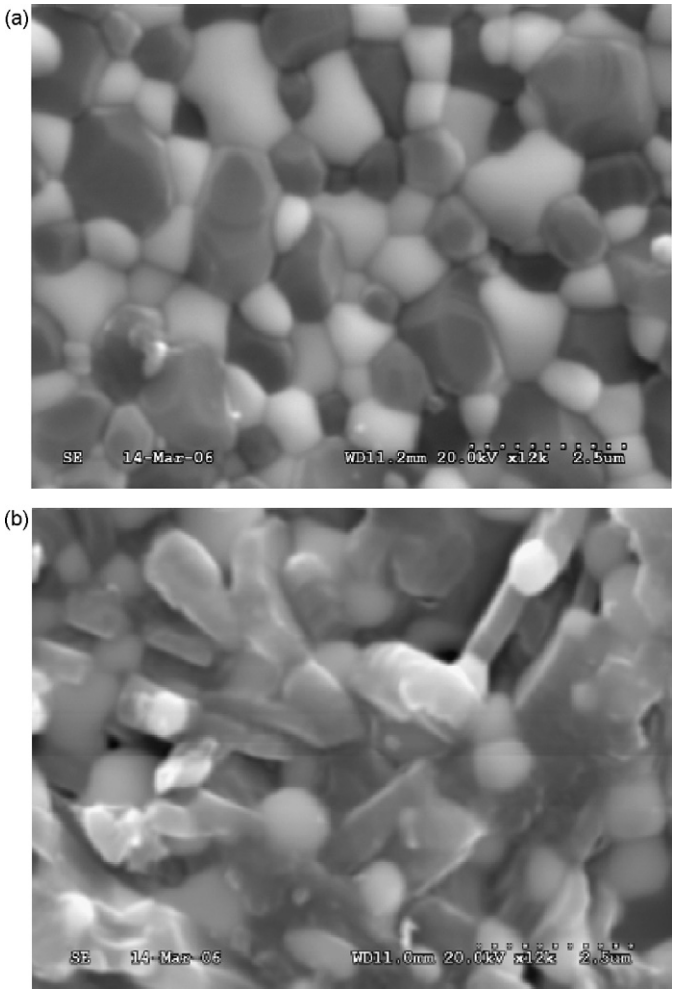

Fig. 5. SEM images of samples (a) before and (b) after conversion [43].

3.5. Conductivity

The structures of β- and β''-Al_2O_3 (see Section 3.1) enable sodium ions to move freely in conduction planes. The conduction planes have a high proportion of defect sites linked by easily accessible networks. As a result, both β- and β''-Al_2O_3 exhibit a relatively high ionic conductivity that is comparable to electrolyte in aqueous batteries while remaining electronically insulated.

Table 3 lists the typical ionic conductivity of single crystal and polycrystalline β- and β''-Al_2O_3. In general, single crystal materials show much higher conductivity compared to polycrystalline ones. It is probably due to the absence of grain-boundary effect and the anisotropic sodium ion conduction in the β- and β''-Al_2O_3 crystals (sodium ion diffusion occurs exclusively within the conduction planes perpendicular to the *c*-axis, see Fig. 2). The conductivity of $1\,S\,cm^{-1}$ at 300 °C was reported for single crystal β''-Al_2O_3 [51,52], which is almost 5 times of that for polycrystalline β''-Al_2O_3. AC impedance analysis allows separation of bulk conduction from grain-boundary effect [53–56], and one example is shown in Fig. 6 [56]. The measured activation energy for bulk conduction in polycrystalline β-Al_2O_3 was similar to that in single crystal. However, the absolute resistance value for the former was much higher than the latter, due to the anisotropic conduction in β-Al_2O_3 lattice.

Several factors influence the conductivity of polycrystalline β/β''-Al_2O_3, including: (i) composition; (ii) relative proportion of β and β'' phases present; and (iii) microstructure (grain size, porosity, impurities, etc.). The effect of composition on the conductivity is most straight-forward. As mentioned earlier, for undoped and doped β-Al_2O_3, the accommodation of excessive sodium atoms in

Table 3
Ionic conductivity of single crystal and polycrystalline β- and β″-Al_2O_3.

	σ (S cm^{-1})		E_a (eV)	Reference
	25 °C	300 °C		
Single crystal β-Al_2O_3	0.036	–	–	[100]
	0.024	–	0.16	[101]
	0.035	0.21	0.13	[56]
	0.03	–	0.16	[102]
	0.014	–	0.16	[103]
	0.03	–	0.17	[15]
	0.025	–	0.15	[104]
	0.03	0.27	0.14	[105]
Polycrystalline β-Al_2O_3	0.0012	0.065	0.27 (25–200 °C) 0.15 (>200 °C)	[56]
Single crystal β″-Al_2O_3	0.04	–	0.22 (25–250 °C) 0.17 (250–650 °C)	[15]
	0.1	–	0.20 (−80 to 150 °C) 0.12 (150–500 °C)	[104]
	0.014	–	0.31 (−80 to 150 °C) 0.09 (150–500 °C)	[104]
	–	1	0.33 (25–150 °C) 0.10 (>150)	[51]
	0.01	1	0.33 (<200 °C)	[52]
Polycrystalline β″-Al_2O_3	–	0.22–0.35	0.15–0.26	[11]
	–	0.21	0.24 (285–330 °C) 0.22 (330–375 °C)	[10]
	–	0.36	0.18 (285–330 °C) 0.16 (330–375 °C)	[10]
	–	0.2	–	[58]

the interstitial sites could significantly improve the conductivity. In the case of doped β-Al_2O_3, the structure change to β″-Al_2O_3 offers accommodation of higher levels of sodium, further increasing the conductivity. Fig. 7 shows an approximately linear relationship between the resistance and proportion of β and β″ phases [12]. Similar observation was reported by Youngblood et al. [11]. Pure β″ phase, therefore, appears to be the most desired phase. However, the relatively low mechanical strength and moisture sensitivity prohibit it to be used solely as electrolyte material. In practical, a two-phase mixture of either β plus β″-Al_2O_3 or ZrO_2-incorporated β″-Al_2O_3 is preferable for good conductivity along with satisfactory mechanical properties. Like mechanical strength, the conductivity of polycrystalline β″-Al_2O_3 is significantly affected by microstructure. The smaller average grain size, the higher fracture strength, but lower conductivity [57–59]. Whalen et al. [58] studied the resistivity and fracture strength of polycrystalline β″-Al_2O_3 as a function of sintering time. A holding time of 15–20 min at 1585 °C was found for optimized microstructure, mechanical strength and conductivity. The presence of impurities also influences the conductivity of β/β″-Al_2O_3. Calcium and silicon are the typical contaminants in ceramic electrolytes. The presence of calcium in β-Al_2O_3 electrolyte led to formation of intergranular calcium aluminate phases, which were likely to block ion transport and cause exponential increase in resistance [60]. The impurity of calcium in the electrolyte might also cause incomplete wetting of electrolyte by liquid sodium anode, which will be discussed in Section 4. The addition of small amounts of silica showed a similar trend of resistance increase due to formation of glassy sodium aluminosilicate phases at triple grain junctions [61].

While potentially enhancing the mechanical strength, the addition of ZrO_2 into β″-Al_2O_3 might deteriorate the electrical performance due to its poor sodium-ionic conductivity. Heavens [49] studied strength improvement in β″-Al_2O_3 with the addition of ZrO_2. It was found that the amounts of ZrO_2 could be up to 10 wt% (~6 vol%) before significant increase in resistivity was observed, as shown in Fig. 8. The resistance of β″-Al_2O_3 with the addition of various amounts of ZrO_2 can be referred to Table 2. Even though the resistance is almost 50% higher compared to that of pure β″-Al_2O_3 (see Table 3), it remains less than 10 Ω cm at 300 °C with up to 15 vol% ZrO_2 addition.

4. Anode

To fully utilize the advantage of sodium anode, the cell has to be structured in a way that can maintain good contact between sodium and BASE during cell operation and keeps sodium/BASE interfacial polarization at a minimum throughout the cell life. There are three common ways to achieve good contact between the anode and BASE: feeding sodium by gravity from a top reservoir, wicking sodium to the BASE surface and forcing sodium from a reservoir by gas pressure. The three designs are schematically shown in Fig. 9. Feeding sodium from a top reservoir is most straight-forward, but it incurs sealing problem due to the contact and possible reaction between the molten sodium and seals, lower sodium utilization rate since redundant sodium has to be maintained in the electrolyte tube even when the cell is fully discharged, and the need for additional space for the excessive sodium and sodium reservoir. The design with a sodium reservoir can be replaced by using metal wicks, such as shims, gauzes and metal foams (see Fig. 9b). Under capillary force, the molten sodium is wicked to the full surface of the BASE and wets it, which is almost independent of the sodium amount in the anode chamber. The wick system exhibits a few advantages over the reservoir design: (i) cost reduction; (ii) simplification in sealing since there is no contact between the molten sodium and seals if the cell is operated vertically; (iii) higher sodium utilization as there is no requirement for excessive sodium; and (iv) more compact cell design. The third method to enhance sodium contact with BASE is pressurizing sodium with an inert gas in a pressure can system (see Fig. 9c). The design gives a simple resolution of cell assembly with a small reduction in specific energy and is more suitable for large vertical cells.

Polarization at the sodium anode and BASE interface manifests itself in a number of ways, including non-linear *I–V* curve, asymmetry of resistance (i.e., lower on charge than on discharge), high transient resistance at the start of discharge or after a period at open circuit, and rapid increase in cell resistance during cycling

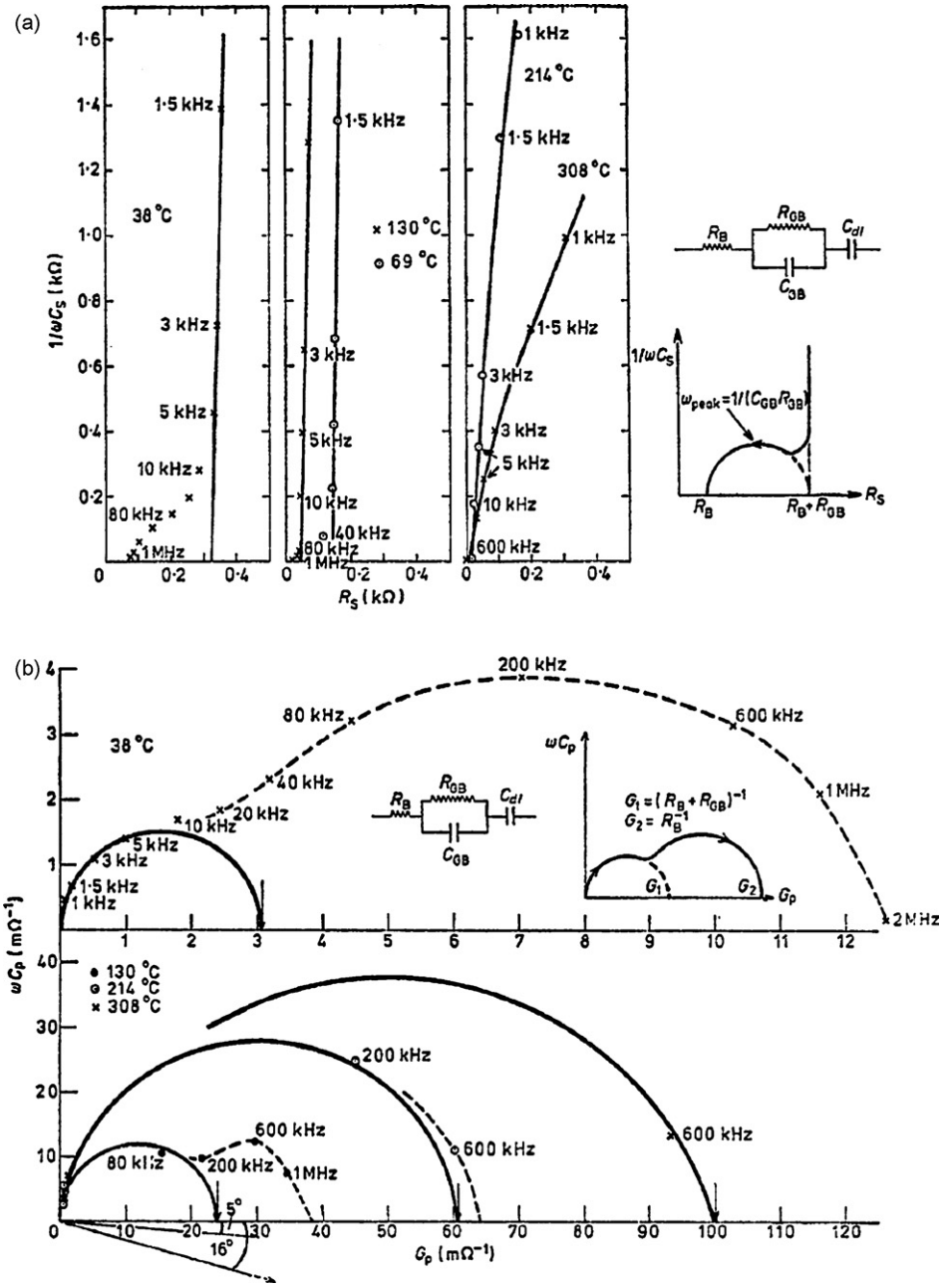

Fig. 6. Impedance and the corresponding admittance plots for polycrystalline β-Al_2O_3 [56]. A simple equivalent circuit model was employed to determine bulk resistance (R_B), electrolyte/electrode interface capacitance (C_{dl}), and parallel combination of a grain-boundary resistance (R_{GB}) and a capacitance (C_{GB}).

[62–64]. Demott [64] observed increase in cell resistance during cycling and found that it could be eliminated by renewal of sodium in the electrode chamber. Not only was the subsequent discharge resistance lower than that prior to renewal, but it remained constant over a large number of cycles and the non-ohmic effects disappeared as well. These observations are not well understood yet. But incomplete wetting of BASE by sodium was identified to be one crucial factor. The incomplete wetting is likely caused by impurities at the sodium anode/BASE interface. As reported by a number of researchers, the addition of small amounts of calcium in the starting powders led to a significant increase in resistivity of the final product during BASE fabrication [39,60,65]. The mobility of calcium was observed by Demott et al. [66] via addition of radioactive Ca-45 into sulfur electrode of Na–S battery. After cycling, a high level of calcium was observed on BASE surface adjacent to sodium electrode. Calcium might be oxidized and form a surface film, which impedes the sodium dissolution as well as sodium ion transport, and eventually causes the observed abnormal in cell resistivity. The wetting of BASE can be modified via treatments of both electrolyte and liquid sodium electrode. Coating the electrolyte surface with a thin layer of lead was proved to significantly decrease contact angle and improve initial wettability of sodium accordingly [66,67]. The ceramic electrolyte surface can be coated with lead acetate by dipping into the corresponding saturated aqueous solution. The lead acetate is then decomposed to metallic lead in a subsequent heat treatment. It was proposed that the treatment with lead might result in calcium oxide dispersed over an increased surface area, and its interference with sodium ion transport was then lessened. Another treatment is addition of titanium or aluminum into the liquid sodium, which serves as oxygen getters to minimize the amount of calcium oxidized at the interface [66,68]. The combination of both treatments was demonstrated to completely eliminate the

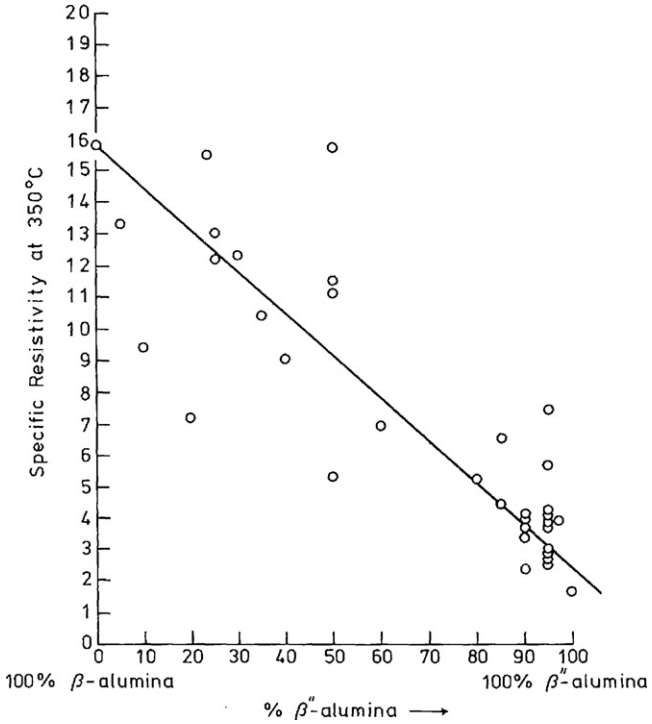

Fig. 7. Resistivity of β-Al_2O_3 as a function of β/β″ ratio [12].

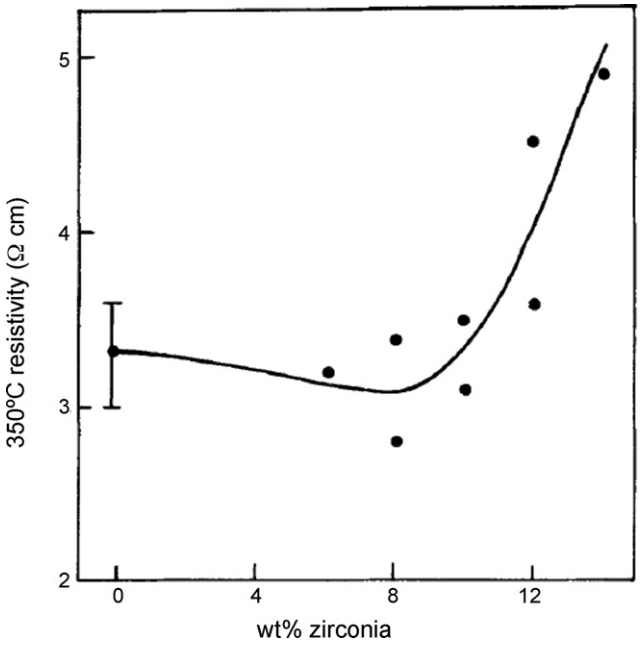

Fig. 8. Effect of ZrO_2 amounts on the resistivity of β″-Al_2O_3 at 350 °C [49].

interfacial effects. The negative effects of calcium oxide at the interface can also be alleviated by modification of the composition of the electrolyte [69]. It was found that, with the doping levels of Li^+ and Na^+ below certain values, the rise in cell resistance could be dramatically suppressed. In addition to the impurities at the interface, Breiter et al. [63] and Viswanathan and Virkar [70] reported sodium reaction with moisture to form a surface layer of sodium oxide, which might be responsible for the incomplete wetting of BASE.

5. Cathode

5.1. Sulfur

The Na–S chemistry offers attractive features such as high theoretical specific energy (~760 Wh kg^{-1}), high energy efficiency and good cycle life. However, sulfide melts are highly corrosive; the material selection for cathode current collector is rather challenging. The use of metals or alloys includes molybdenum, chromium as well as some alloys, and inexpensive materials such as stainless steels are limited due to corrosion [71]. Degradation of BASE in the corrosive melt was also reported [72]. In addition, both sulfur and sodium polysulfide are electrical insulators. As such, graphite felt is typically used in the cathode as a current collector, which incurs high cost. Another critical issue with the Na–S battery is its cell failure mode. When BASE is broken, the sulfide melts are in direct contact with liquid sodium; reaction between them is inherently vigorous, potentially causing fire and even explosion due to temperature excursion since the cell operation temperature (300–400 °C) is close to the boiling point of sulfur (440 °C). Furthermore, as the cell fails, resistance increases significantly and renders the entire series of cells open-circuited.

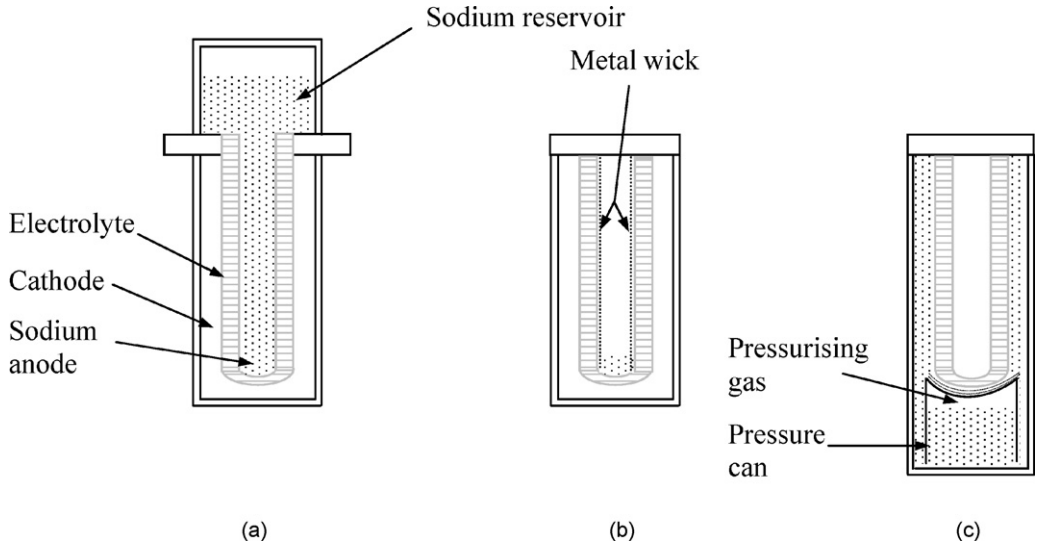

Fig. 9. Schematic of three anode designs in tubular cell.

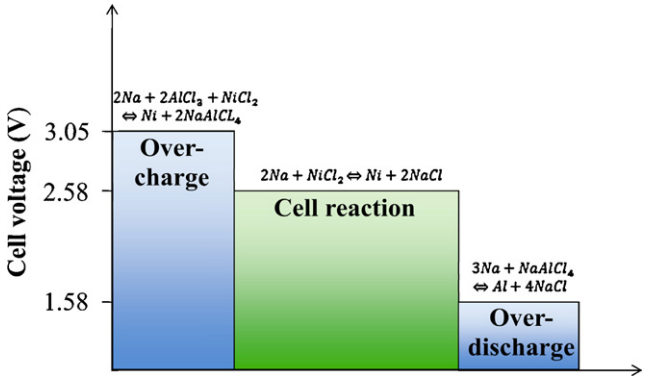

Fig. 10. Cell reactions in sodium battery using nickel chloride cathode at 300 °C.

5.2. Transition metal halides

Alternatively, metal halides can be employed to replace sulfur in NBB cathodes. $SbCl_3$ [73], Cl_2 [74] and SCl^{3+} [75] were first examined. In spite of their attractive energy density, these materials are not free from corrosion problems. In 1986, a new class of sodium battery system was reported in ZEBRA cells that employed transition metal chlorides as solid cathodes in a secondary molten electrolyte of $NaAlCl_4$ (melting point, 170 °C) [76]. The secondary molten electrolyte serves mostly as a sodium ion transport medium between BASE and reaction zone in the cathode and does not participate in the cathode reaction. Thus, composition and conductivity of the $NaAlCl_4$ melt remain unchanged during charge/discharge. The metal halide cathodes are less corrosive than sodium polysulfide in Na–S battery, easing materials selection for current collectors and cell container. The electrochemical cell is typically assembled in a discharged state without the need of handling metallic sodium. Transition metals, such as nickel or iron, and sodium chloride as starting materials are mixed and filled into the cathode chamber to form a porous matrix. Then, the molten $NaAlCl_4$ is vacuum-impregnated into the porous cathode to extend the reaction zone. Another major advantage of the system over Na–S battery is the low resistance cell failure mode. If BASE is broken, liquid $NaAlCl_4$ reacts with sodium to generate sodium chloride as well as metallic aluminum. The reaction is much less violent compared to that in Na–S battery. Small cracks in BASE can be resealed by the reaction products. In the case of large cracks, the produced aluminum shorts the current pathway between the anode and cathode and eventually leads to a low cell resistance. The entire battery can be further operated with only loss of voltage associated with the broken cell and without loss of ampere-hour capacity. Another advantage of the ZEBRA batteries is their tolerance to overcharge and overdischarge. For example, if made from Ni and NaCl (see Fig. 10), the cathode can be excessively charged at a higher voltage than the normal charge with the cost of current collector and $NaAlCl_4$ melt, which can serve as a useful "end of charge" indicator so that the risk of BASE breakdown can be avoided. The overdischarge reaction, which is similar to the cell failure reaction, happens at a much lower voltage without an electrolyte failure. One notable disadvantage of the current ZEBRA technology is its lower power than the Na–S battery.

5.2.1. Nickel chloride

A critical requirement for cathode materials is that their electrochemically active species must be insoluble in $NaAlCl_4$ melt in both charged and discharged states. Thus, mass transport of the species to BASE surface and potential ion exchange with sodium in the electrolyte could be prevented. So far, among various transition metal chlorides, nickel [4,5] and ferrous [77,78] chlorides meet the requirement and have been extensively studied. As seen in Eqs. (4)–(6), the half- and overall-cell reactions for nickel chloride cathodes are rather simple. The open-circuit voltage of the cell is 2.59 V at 250 °C, which is 0.24 V higher compared to that of ferrous chloride cathodes. A number of studies have been carried out to understand the charge/discharge processes and improve the performance of nickel chloride cathodes [5,79–86]. A low-conducting layer of nickel chloride was reported to form on the nickel surface during charge. Once it reached a certain thickness (on the order of one micrometer), further charge of the cell was suppressed. As a result, both utilization of the electrode and cell capacity were limited [83,86]. The solubility of nickel chloride in $NaAlCl_4$ melt at elevated temperatures is another issue. Redey et al. [87] pointed out that a higher concentration of nickel ions in the melt could exchange with sodium ions in BASE, resulting in a lower conductivity and premature failure of the electrolyte. The third problem is capacity loss during cycling. Bones et al. [5] studied stability of cell with nickel chloride cathode and observed capacity decreased by ~50% in less than 10 cycles. The loss was diagnosed to be related to growth of nickel grains within the cathode during cycling. Modification of the molten electrolyte and porous cathode with certain chemical additives has been carried out to minimize the degradation in capacity. Prakash et al. [86] reported the addition of small amounts of sodium bromide, sodium iodide and sulfur into the molten electrolyte, that led to much higher nickel utilization and lower impedance. It was believed that formation of nickel bromide and nickel iodide, which have larger lattice parameters than nickel chloride, eased ion transport in the cathode layer during charge/discharge processes and therefore enhanced the capacity. Other study suggested the enhanced capacity from combination effects of sodium bromide addition into cathode and sodium iodide and sulfur addition into molten electrolyte [83]. A further study by Prakash et al. [86] found that the addition of sodium bromide, sodium iodide and sulfur into the molten electrolyte could dramatically reduce the solubility of nickel chloride in the melt. The addition of 1–5 wt% sulfur into the melt was also observed to dramatically suppress the coarsening of nickel grains during cycling. The cell with sulfur-doped nickel chloride cathode was demonstrated to have a long cell life (>2000 cycles) with capacity retention >75% and negligible resistance increase [5]. Other solutions to improve cell performance include incorporation of small amounts of aluminum, iron and iron sulfide into the nickel chloride electrode [88,89]. In addition to the composition modification, electrode morphology can also significantly affect the cell performance. Prakash et al. [85] investigated electrochemical properties of nickel chloride electrode with three morphologies: a nonporous nickel substrate, a nickel felt and a porous sintered electrode. It was found that there was a direct relationship between the electrochemical performance and morphological parameters (BET area and pore-size distribution). Significant enhancement in performance was achieved with the porous sintered electrode. Cell performance improvement with the addition of pore-former was reported as well [83]. The nickel chloride cathode can be fabricated by various methods, including: (i) impregnation of nickel chloride into a sintered nickel grid [80,81]; (ii) impregnation or physical vibrating sodium chloride into a nickel felt to form an electrode in the discharged state [85]; or (iii) cosintering of sodium chloride and nickel powders at high temperatures (~700 °C) in an inert atmosphere [5,83–85].

5.2.2. Ferrous chloride

At relatively low cost, ferrous chloride is a popular cathode material for ZEBRA batteries [77,78,90–92]. Similar to the sodium/nickel chloride couple, sodium/ferrous chloride cathode shows a preferred operating voltage range (see Fig. 11). If discharge continues with no more ferrous chloride available in the cathode, sodium ions react with aluminum chloride component in

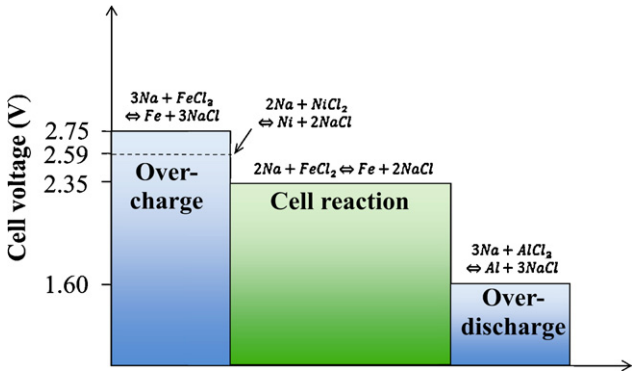

Fig. 11. Cell reactions in sodium battery using ferrous chloride cathode at 250 °C.

the molten electrolyte to produce metallic aluminum as well as sodium chloride, and the cell voltage immediately drops to 1.6 V. The reaction is reversible and only consumes molten electrolyte, which is similar to the overdischarge reaction of sodium/nickel chloride couple. However, during abuse of overcharge, as seen in Fig. 11, remnant iron in the cathode reacts with sodium chloride component in the melt at a higher voltage (i.e., 2.75 V). The overcharge reaction is extremely undesirable because it causes: (i) formation of ferric chloride, which is soluble even in the basic $NaAlCl_4$ melt and might transport and penetrate into the electrolyte; and (ii) depletion of sodium chloride in the melt, resulting in an acidic aluminum chloride-rich melt. Both of them eventually lead to degradation of the electrolyte. Moseley et al. [78] studied stability of BASE in the sodium/ferrous chloride cell and observed that surface layer of the electrolyte adjacent to the cathode compartment was physically damaged and iron ions penetrated into the layer during overcharge. The damage of the surface layer was probably caused by ferric chloride or excessive aluminum chloride in the $NaAlCl_4$ melt while ion penetration only appeared with an applied electric field. In short, the sodium/ferrous chloride cell is sensitive to overcharge. To overcome the problem, a small amount of nickel metal (with extra sodium chloride) is incorporated into the cathode. As shown in Fig. 11, the overcharge reaction can now be replaced with oxidation of nickel to insoluble nickel chloride without either depleting the sodium chloride in the melt or oxidizing the iron metal to ferric chloride. Another issue is related to degradation of cell performance at elevated temperatures. In the same paper, iron ions were observed to penetrate into BASE during the regular charge/discharge at higher temperatures (e.g., 370 °C), which caused a significant increase in cell resistance [78]. It was likely due to increased solubility of iron species in the melt at these temperatures. The addition of sodium fluoride, similar to the additives of sodium bromide, sodium iodide and sulfur into nickel chloride cathode, can effectively inhibit the access of iron ions into the electrolyte [76,78]. Meanwhile, it is suggested that the cell operates at temperatures below 300 °C to avoid overheated.

5.2.3. Others

In addition to nickel and ferrous chlorides, a number of other transition metal chlorides have been extensively examined by Ratnakumar et al. [81,93] as potential cathode materials. The salts studied include copper, manganese, chromium, aluminum, silver, titanium, molybdenum and cobalt chlorides. Among them, only molybdenum and cobalt chlorides appeared to be insoluble in the molten electrolyte and promising as the cathode materials. Virkar et al. [42,43] explored the possibility of using zinc chloride and tin (IV) iodide as cathodes. Immersion test with BASE in the corresponding molten salts revealed no ion exchange occurred. However, based on the previous discussion and reports [94], the presence of an applied electric field likely affects the ion exchange behavior. Apparently, more work is needed to clarify it.

6. Perspectives

Owing to the excellent properties such as high theoretical energy density, high round-trip efficiency and good cycle life, NBBs have gained great interests for stationary and transportation applications. However, broad market penetration requires further advancement in performance, safety and cost reduction via use of new materials along with novel component/cell designs and engineering.

One trend is to reduce operating temperatures so that can allow for improvement in materials durability, use of more cost-effective cell and stack materials, and ease thermal management. This may require optimization of current electrolytes or development of alternative sodium ion conductors (e.g., NASICON [95,96]) that can demonstrate facile sodium ion transport at the reduced temperatures. In addition, the reduction in operating temperatures may call for new cathodes that can demonstrate satisfactory electrochemical activities at the reduced temperatures. The reduction in operating temperatures can also open a door to employ organic materials such as ionic liquids in the electrodes. There has been limited efforts [80,97] involving tetracyanoethylene (TCNE) as cathode, which exhibited an energy density as high as 620 Wh kg^{-1} with a potential of ~3.0 V versus Na^+/Na (but had issues for practical use).

Alternatively, introduction of novel designs, along with the use of new materials and materials/component fabrication, can help meet performance and cost requirements. The tubular design has been the dominate geometry of NBBs since the invention. ZEBRA cell was optimized with the cross section from round to clover leaf shape BASE [88,89], which significantly increased the available electrolyte surface area, reduced the thickness of cathode and eventually improved power density of the cell. Recently, planar electrolyte has been considered [98,99]. The US Department of Energy's ARPA-E program has announced funding of planar sodium-beta battery development effort proposed by EaglePitcher Technologies, LLC and the Pacific Northwest National Laboratory. The drastic changes in design potentially lead to improved energy/power densities and ease manufacturing. To fully utilize the advantages of the novel designs, however, robust, effective seals along with other components or materials have to be developed. Overall, substantial progress demands the use of new materials/chemistries and radical changes in designs and engineering.

Acknowledgements

The work is supported by Laboratory-Directed Research and Development Program (LDRD) of the Pacific Northwest National Laboratory (PNNL), the US Department of Energy's Advanced Research Projects Agency-Energy (ARPA-E), and Office of Electricity Delivery & Energy Reliability's storage program. PNNL is a multiprogram laboratory operated by Battelle Memorial Institute for the US Department of Energy under Contract DE-AC05-76RL01830.

References

[1] http://www.electricitystorage.org/site/technologies/.
[2] J.T. Kummer, N. Weber, U.S. Patent 3,413,150 (1968).
[3] J.T. Kummer, in: H. Reiss, J.O. McCaldin (Eds.), Beta-Alumina Electrolytes, Pergamon Press, New York, 1972, pp. 141–175.
[4] R.C. Galloway, J. Electrochem. Soc. 134 (1987) 256.
[5] R.J. Bones, D.A. Teagle, S.D. Brooker, F.L. Cullen, J. Electrochem. Soc. 136 (1989) 1274.
[6] W.L. Bragg, C. Gottfried, J. West, Z. Kristallogr. 77 (1931) 255.
[7] C.A. Beevers, M.A.S. Ross, Z. Kristallogr. 97 (1937) 59.
[8] G. Yamaguch, K. Suzuki, Bull. Chem. Soc. Japan 41 (1968) 93.

[9] M. Bettman, C.R. Peters, J. Phys. Chem. 73 (1969) 1774.
[10] A.V. Virkar, G.R. Miller, R.S. Gordon, J. Am. Ceram. Soc. 61 (1978) 250.
[11] G.E. Youngblood, G.R. Miller, R.S. Gordon, J. Am. Ceram. Soc. 61 (1978) 86.
[12] J.L. Sudworth, A.R. Tilley, The Sodium Sulphur Battery, Chapman & Hall, London, 1985.
[13] W.L. Roth, F. Reidinger, S.J. Laplaca, in: G.D. Mahan, W.L. Roth (Eds.), Superionic Conductors, Plenum Press, New York, 1976, p. 223.
[14] J.C. Wang, M. Gaffari, S. Choi, J. Chem. Phys. 63 (1975) 772.
[15] N. Baffier, J.C. Badot, P. Colomban, Mater. Res. Bull. 16 (1981) 259.
[16] A.K. Ray, E.C. Subbarao, Mater. Res. Bull. 10 (1975) 583.
[17] Y. Sheng, P. Sarkar, P.S. Nicholson, J. Mater. Sci. 23 (1988) 958.
[18] T. Oshima, M. Kajita, A. Okuno, Int. J. Appl. Ceram. Technol. 1 (2004).
[19] P. Morgan, Mater. Res. Bull. 11 (1976) 233.
[20] B.E. Yoldas, D.P. Partlow, Am. Ceram. Soc. Bull. 59 (1980).
[21] J.D. Hodge, Am. Ceram. Soc. Bull. 62 (1983) 244.
[22] M. Zaharescu, C. Parlog, V. Stancovschi, D. Crisan, A. Braileanu, T. Surdeanu, Solid State Ionics 15 (1985) 55.
[23] S. Yamaguchi, K. Terabe, Y. Iguchi, A. Imai, Solid State Ionics 25 (1987) 171.
[24] V. Jayaraman, T. Gnanasekaran, G. Periaswami, Mater. Lett. 30 (1997) 157.
[25] T. Takahashi, K. Kuwabara, J. Appl. Electrochem. 10 (1980) 291.
[26] A. Pekarsky, P.S. Nicholson, Mater. Res. Bull. 15 (1980) 1517.
[27] D.J. Green, S. Hutchison, Mater. Sci. Monogr. 6 (1980) 964.
[28] A.D. Jatkar, I.B. Cutler, R.S. Gordon, in: R.M. Fulrath, J.A. Pask (Eds.), Ceramic Microstructures, Westview Press, Boulder, CO, 1978, p. 414.
[29] J.H. Duncan, W.G. Bugden, Proc. Br. Ceram. Soc. 31 (1981) 221.
[30] G.E. Youngblood, A.V. Virkar, W.R. Cannon, R.S. Gordon, Am. Ceram. Soc. Bull. 56 (1977) 206.
[31] A. Vanzyl, M.M. Thackeray, G.K. Duncan, A.I. Kingon, R.O. Heckroodt, Mater. Res. Bull. 28 (1993) 145.
[32] A. vanZyl, Solid State Ionics 86–88 (1996) 883.
[33] C.N. Poulieff, R. Kvachkov, I.M. Balkanov, Mater. Res. Bull. 13 (1978) 323.
[34] J.H. Kennedy, A. Foissy, J. Electrochem. Soc. 122 (1975) 482.
[35] R.W. Powers, J. Electrochem. Soc. 122 (1975) 490.
[36] W. Byckalo, G. Rosenblatt, J. Lam, P.S. Nicholson, Am. Ceram. Soc. Bull. 55 (1976) 286.
[37] M. Rivier, A.D. Pelton, Am. Ceram. Soc. Bull. 57 (1978) 183.
[38] Ford Motor Company, British Patent 1,541,850 (1979).
[39] I.W. Jones, L.J. Miles, Proc. Br. Ceram. Soc. 19 (1971) 161.
[40] A.D. Jatkar, I.B. Cutler, R.S. Gordon, in: R.M. Fulrath, J.A. Pask (Eds.), Ceramic Microstructures, Westview Press, Boulder, Colorado, 1976, p. 412.
[41] A.V. Virkar, J.-F. Jue, K.-Z. Fung, U.S. Patent 6,117,807.
[42] P. Parthasarathy, N. Weber, A.V. Virkar, ECS Trans. 6 (2007) 67.
[43] A.V. Virkar, A high temperature electrochemical energy storage system based on sodium beta″-alumina solid electrolyte (BASE), report to DOE, 2008.
[44] F.F. Lange, B.I. Davis, D.O. Raleigh, J. Am. Ceram. Soc. 66 (1983) C50.
[45] L. Viswanathan, Y. Ikuma, A.V. Virkar, J. Mater. Sci. 18 (1983) 109.
[46] D.J. Green, M.G. Metcalf, Am. Ceram. Soc. Bull. 63 (1984) 803.
[47] J.G.P. Binner, R. Stevens, J. Mater. Sci. 20 (1985) 3119.
[48] D.J. Green, J. Mater. Sci. 20 (1985) 2639.
[49] S.N. Heavens, J. Mater. Sci. 23 (1988) 3515.
[50] A.V. Virkar, J. Mater. Sci. 16 (1981) 1142.
[51] H. Engstrom, J.B. Bates, W.E. Brundage, J.C. Wang, Solid State Ionics 2 (1981) 265.
[52] J.B. Bates, H. Engstrom, J.C. Wang, B.C. Larson, N.J. Dudney, W.E. Brundage, Solid State Ionics 5 (1981) 159.
[53] G.C. Farringt, J. Electrochem. Soc. 121 (1974) 1314.
[54] R.D. Armstrong, T. Dickinson, P.M. Willis, J. Electroanal. Chem. 53 (1974) 389.
[55] R.W. Powers, S.P. Mitoff, J. Electrochem. Soc. 122 (1975) 226.
[56] A. Hooper, J. Phys. D: Appl. Phys. 10 (1977) 1487.
[57] A.V. Virkar, G.J. Tennenhouse, R.S. Gordon, J. Am. Ceram. Soc. 57 (1974) 508.
[58] T.J. Whalen, G.J. Tennenhouse, C. Meyer, J. Am. Ceram. Soc. 57 (1974) 497.
[59] A.V. Virkar, R.S. Gordon, J. Am. Ceram. Soc. 60 (1977) 58.
[60] A.C. Buechele, L.C. De Jonghe, Am. Ceram. Soc. Bull. 58 (1979) 861.
[61] M.Y. Hsieh, L.C. De Jonghe, J. Am. Ceram. Soc. 61 (1978) 185.
[62] J.L. Sudworth, A.R. Tilley, K.D. South, in: W. van Gool (Ed.), Fast Ion Transport in Solids, North-Holland, Amsterdam, 1973, p. 581.
[63] M.W. Breiter, B. Dunn, R.W. Powers, Electrochim. Acta 25 (1980) 613.
[64] D.S. Demott, J. Electrochem. Soc. 127 (1980) 2312.
[65] A. Imai, M. Harata, Jpn. J. Appl. Phys. 11 (1972) 180.
[66] D.S. Demott, M.L. Wright, M.D. Hames, Ext. Abstr. No. 469, Electrochem. Soc. Meet. (1981).
[67] M.L. Wright, British Patent Application 2,067,005 (1981).
[68] M.L. Wright, M.D. Hames, British Patent Application 2,080,608 (1982).
[69] W.G. Bugden, P. Barrow, J.H. Duncan, Solid State Ionics 5 (1981) 275.
[70] L. Viswanathan, A.V. Virkar, J. Mater. Sci. 17 (1982) 753.
[71] R.P. Tischer, The Sulphur Electrode, Academic Press, New York, 1983.
[72] M. Liu, Degradation of sodium β″ alumina electrolyte in contact with sulfur/sodium polysulfide melts, Lawrence Berkeley Laboratory, report, 1986, LBL-21563.
[73] N.P. Yao, J.R. Selman, Proceedings of the Symposium on Load Leveling, The Electrochemical Society Softbound Proceedings Series, Princeton, NJ, 1977.
[74] J.J. Werth, U.S. Patent 3,847,667 (1974); U.S. Patent 3,877,984 (1975).
[75] G. Mamantov, R. Marassi, M. Matsunga, Y. Ogata, J.P. Wiaux, E.J. Frazer, J. Electrochem. Soc. 127 (1980) 2319.
[76] J. Coetzer, J. Power Sources 18 (1986) 377.
[77] R.J. Bones, J. Coetzer, R.C. Galloway, D.A. Teagle, J. Electrochem. Soc. 134 (1987) 2379.
[78] P.T. Moseley, R.J. Bones, D.A. Teagle, B.A. Bellamy, R.W.M. Hawes, J. Electrochem. Soc. 136 (1989) 1361.
[79] B.V. Ratnakumar, S. Distefano, G. Halpert, J. Electrochem. Soc. 137 (1990) 2991.
[80] S. Distefano, B.V. Ratnakumar, C.P. Bankston, J. Power Sources 29 (1990) 301.
[81] B.V. Ratnakumar, A.I. Attia, G. Halpert, J. Power Sources 36 (1991) 385.
[82] B.V. Ratnakumar, S. Distefano, C.P. Bankston, U.S. Patent 5,019,470 (1991).
[83] L. Redey, D.R. Vissers, J. Prakash, U.S. Patent 5,283,135 (1994); U.S. Patent 5,340,668 (1994).
[84] L. Redey, D.R. Vissers, J. Prakash, K.M. Myles, U.S. Patent 5,532,078 (1996); U.S. Patent 5,536,593 (1996).
[85] J. Prakash, L. Redey, D.R. Vissers, J. Power Sources 84 (1999) 63.
[86] J. Prakash, L. Redey, D.R. Vissers, J. Electrochem. Soc. 147 (2000) 502.
[87] L. Redey, C. Rose, R. Lowrey, Ext. Abstr., Electrochem. Soc. Meet. (1992).
[88] R.C. Galloway, S. Haslam, J. Power Sources 80 (1999) 164.
[89] J.L. Sudworth, J. Power Sources 100 (2001) 149.
[90] J. Coetzer, G.D. Wald, S.W. Orchard, J. Appl. Electrochem. 23 (1993) 790.
[91] K.T. Adendorff, M.M. Thackeray, J. Electrochem. Soc. 135 (1988) 2121.
[92] S.W. Orchard, J.S. Weaving, J. Appl. Electrochem. 23 (1993) 1214.
[93] B.V. Ratnakumar, A.I. Attia, G. Halpert, J. Electrochem. Soc. 138 (1991) 883.
[94] R. Roumieu, A.D. Pelton, J. Electrochem. Soc. 128 (1981) 50.
[95] J.B. Goodenough, H.Y.P. Hong, J.A. Kafalas, Mater. Res. Bull. 11 (1976) 203.
[96] H.Y.P. Hong, Mater. Res. Bull. 11 (1976) 173.
[97] B.V. Ratnakumar, S. Distefano, R.M. Williams, G. Nagasubramanian, C.P. Bankston, J. Appl. Electrochem. 20 (1990) 357.
[98] J.L. Sudworth, M.D. Hames, M.A. Storey, M.F. Azim, A.R. Tilley, in: D.H. Collins (Ed.), Power Sources, vol. 4, Oriel Press, Newcastle Upon Tyne, UK, 1973, p. 1.
[99] H.P. Silverman, T.R.W. development program for solid electrolyte batteries, E.P.R.I. Rep. EM-266, project 127, 1976.
[100] R.D. Armstrong, T. Dickinson, P.M. Willis, J. Electroanal. Chem. 67 (1976) 121.
[101] W.L. Fielder, H.E. Kautz, J.S. Fordyce, J. Singer, J. Electrochem. Soc. 122 (1975) 528.
[102] Y.F.Y. Yao, J.T. Kummer, J. Inorg. Nucl. Chem. 29 (1967) 2453.
[103] Ms. Whitting, R.A. Huggins, J. Chem. Phys. 54 (1971) 414.
[104] J.L. Briant, G.C. Farrington, J. Solid State Chem. 33 (1980) 385.
[105] H. Engstrom, J.B. Bates, J.C. Wang, Solid State Commun. 35 (1980) 543.